Developmental clock and mechanism of *de novo* polarization of the mouse embryo

Meng Zhu[1], Jake Cornwall-Scoones[2], Peizhe Wang[3], Charlotte E. Handford[1,4], Jie Na[3], Matt Thomson[2] and Magdalena Zernicka-Goetz[1,2,4*]

[1] University of Cambridge, Department of Physiology, Development and Neuroscience; Downing Street, Cambridge, CB2 3DY, UK.

[2] California Institute of Technology (Caltech), Division of Biology and Biological Engineering, Pasadena, CA 91125, USA.

[3] Centre for Stem Cell Biology and Regenerative Medicine, School of Medicine, Tsinghua University, Beijing, 100084, China.

[4] Centre for Trophoblast Research, University of Cambridge, Cambridge, CB2 3EG

* corresponding author: mz205@cam.ac.uk

Embryo polarization is critical for mouse development; however, neither the regulatory clock nor the molecular trigger that it activates are known. Here, we show that the embryo polarization clock reflects the onset of zygotic genome activation, and we identify three factors required to trigger polarization. Advancing the timing of Tfap2c and Tead4 expression in the presence of activated RhoA induces precocious polarization as well as subsequent cell fate specification and morphogenesis. Tfap2c and Tead4 induce expression of actin regulators that control the recruitment of apical proteins on the membrane, whereas RhoA regulates their lateral mobility, allowing the emergence of the apical domain. Thus, Tfap2c, Tead4, and RhoA are regulators for the onset of polarization and cell fate segregation in the mouse.

Introduction

The totipotent mammalian zygote can produce any embryonic or extra-embryonic tissue but this becomes restricted in the first cell fate decision that generates distinct inner cell mass (ICM) and outer extra-embryonic trophectoderm (TE). The ICM will form epiblast (EPI) and extra-embryonic primitive endoderm (PE), generating the future fetus and the yolk sac, respectively. The TE will form the placenta. Formation of these three lineages by implantation is a prerequisite for successful pregnancy.

Embryo polarization is key to the segregation of the ICM and TE lineages (*1, 2*). In the mouse, this process happens at the 8-cell stage (*2-4*) when each blastomere acquires an apical domain, comprising the Par protein complex and ERM proteins (ezrin, radixin and moesin) enclosed by an actomyosin ring (*5, 6*). The apical domain enables expression of transcription factors such as Cdx2 and Gata3, which drive differentiation into TE, whereas apolar cells maintain pluripotency to become ICM (*7, 8*).

Mammalian embryo development is regulative and yet the timing of embryo polarization remains unchanged even if embryos are split into individual blastomeres, when cells are aggregated together, or when cell divisions are prevented. Thus, the polarization seems set to a strict developmental clock that is independent of cell number (*9, 10*). Here, we show that this clock reflects activation of the zygotic genome, and we identify three factors whose convergent activity triggers self-organization of the apical domain.

Critical threshold of transcripts required for embryo polarization

Polarization timing varies between species, reflecting the onset of zygotic-genome-activation (ZGA) (*11, 12*). In mouse, the major wave of ZGA occurs at the 2-cell stage but an additional transcriptional wave occurs at the early 8-cell stage just before polarization (*13*). To determine whether the latter transcriptional wave is associated with polarization, we first treated embryos from the early 8-cell stage with two transcription inhibitors: 5,6-Dichlorobenzimidazole 1-β-D-ribofuranoside DRB and Triptolide. Either drug prevented apical localization of the polarity marker Pard6 (Fig.1A-D; Fig.S1A-G). Polarization was restored by washing-out the reversible transcription inhibitor DRB (Fig.S1H-J). Thus, transcription at the early 8-cell stage appears to be required for embryo polarization. As a second test, we reduced the cytoplasmic volume (Fig.1E), shown by others to increase the concentration of newly synthesized mRNA (*14, 15*). We injected zygotes with an apical marker (Ezrin-RFP mRNA) and resected 30-40% of cytoplasm from one 2- or 4-cell stage blastomere, using a technique that does not compromise development (*16*)(Fig.1F). Single-molecule fluorescence in situ hybridization confirmed that this increased the concentration of newly transcribed mRNAs (*17*)(Fig.S2A-E). Such blastomere resection brought forward embryo polarization by 2.1hr when performed at the 2-cell stage (Fig.1F-I; N=62 pairs; Movie S1) and by 3.3hr at the 4-cell stage (Fig.S2F-H; Fig.1J; N=76 pairs; Movie S2). Both experimental and control embryos had established all three lineages as blastocysts (Fig.S2I-K). Inhibiting transcription with a 3hr pulse of DRB led both resected and control blastomeres to polarize simultaneously (Fig.1K; Fig.S2L-N). These results indicate that *de novo* synthesis of transcripts and their accumulation to a critical threshold is required for embryo polarization.

Tfap2c and Tead4 are required for embryo polarization

We hypothesized that the requirement for 8-cell stage transcription could result from direct expression of cytoskeletal regulators of cell polarization or their indirect expression through a transcriptional hierarchy. We therefore interrogated published single-cell RNA-sequencing data (*18*) and selected genes for 118 cytoskeletal polarity regulators and 6 transcription factors that show increased expression by the 8-cell stage and hence are likely to be active according to ATAC-seq (*19*)(Fig.S3; Table

S1,2). We downregulated each of these 124 genes by RNAi (Fig.S3; Fig.S4A-B) and scored the timing of embryo polarization from time-lapse imaging of the distribution of Ezrin-RFP (Fig.2A-D). Only depletion of the transcription factors Tfap2c or Tead4 prevented embryo polarization (Fig.2A-C,E; Fig.S4A-E). Individual depletion of Tfap2c and Tead4 delayed polarization from the 8- to the 16-cell stage (Fig.2A-C, E-F) whereas polarization was entirely abolished by their co-depletion (Fig.2D-H). Depletion of Tfap2c and Tead4 also prevented precocious polarization resulting from blastomere resection (Fig.S4F-G).

To confirm the requirement for Tfap2c and Tead4 in polarization, we deleted both genes by CRISPR-Cas9 mutagenesis. We designed three sgRNAs to target a single protein-coding exon of each gene (Fig.2I) and injected them into the zygote together with Cas9 mRNA and Ezrin-RFP mRNA as an apical marker. We categorized blastomeres based on whether they had undetectable, moderate, or wild-type levels of Tfap2c or Tead4 proteins at the 8-16-cell stage (Fig.S5A-B) and confirmed by DNA sequencing that blastomeres with undetectable Tfap2c or Tead4 were homozygous mutants (Fig.2J; Fig.S5C-D). Simultaneous deletion of *Tfap2c* and *Tead4* completely abolished embryo polarization, contrasting with their individual deletions that were less severe (Fig.2J-L; Fig.S5E-F). Thus, zygotic expression of *Tfap2c* and *Tead4* is required for embryo polarization at the 8-cell stage.

Previously Tead4 had been previously shown to function only downstream of polarization, following nuclear re-localization of its transcriptional co-activator Yap to induce TE transcription factor expression (*7*). To gain further insight into the earlier role of Tead4, we examined the localization of Yap. We found Yap localization in the nucleus before polarization at the 8-cell stage (*20*)(Fig.S6A-C) that was diminished by downregulation (Fig.S6D-E) and enhanced by upregulation of Tead4 (Fig.S6F-G). Thus, Tead4 affects the localization of Yap before polarization, indicating a previously undescribed, polarity-independent Tead4 function.

Advancing expression of Tfap2c, Tead4, and Rho GTPase advances polarization timing

As we found that Tfap2c and Tead4 are required for embryo polarization, we wished to determine whether advancing their expression would advance the timing of

polarization. We therefore injected Tfap2c and Tead4 mRNAs into one blastomere at the late 2-cell stage, to elevate their expression at the 4-cell stage (Fig.S7A-C). Advancing expression of Tead4 did not induce premature polarization (Fig.S7D-E, I-J). Advancing expression of Tfap2c led to formation of cell protrusions enriched in apical polarity proteins, including Pard6 and Ezrin at the 4-cell stage (Fig.S7F-I). Advancing the expression of Tfap2c and Tead4 together also induced premature formation of protrusions (Fig.S7G-I; Fig.3B-C; Movie S3-4). In all cases, the induced protrusions were smaller than the natural apical domain at the 8-cell stage (Fig.3B; Movie S3-4; Fig.S7H). These results suggested Tfap2c and Tead4 might be sufficient to trigger polarization of apical proteins but other factors are required for proper apical domain formation.

We previously found that actomyosin activation by PKC-Rho GTPase signaling was necessary but not sufficient to trigger apical domain formation (Fig.3B-C, Movie S5) (*21*). We therefore hypothesized that Rho GTPase activation might be required with Tfap2c and Tead4 to achieve complete polarization. To test this, we injected mRNAs for Tfap2c and Tead4 at the 2-cell stage (with Ezrin-RFP mRNA as apical marker) and mRNA for constitutively active RhoA-Q63L at the 4-cell stage (with LifeAct-GFP as injection marker)(Fig.3A; Fig.S7K). Expression of all three factors established complete apical domains at the 4-cell stage (Fig.3B-C; Movie S6). These induced apical domains were enriched with Ezrin and Pard6, strongly resembling apical domains that form normally only at the 8-cell stage (Fig.3B; Fig.S8B-C).

To confirm these results, we overexpressed these factors in just half the embryo and found that the targeted blastomeres polarized earlier than controls in the other embryo half (Fig.3D-F; Movie S7-8). We observed no differences in division timing between blastomeres suggesting induced 4-cell stage polarization is not caused by a cytokinesis delay (Fig.S8A). Together our results indicate that a transcriptional program triggered by Tfap2c and Tead4 alongside activation of actomyosin downstream of Rho GTPase signaling triggers polarization at a specific stage of embryogenesis.

Advancing Tfap2c, Tead4 and Rho GTPase expression advances morphogenesis and differentiation

Embryo polarization at the 8-cell stage is followed by the zippering of adjacent apical domains, which expand and seal their boundaries at the late 16-cell stage to enable blastocyst formation (*22*). To determine whether premature polarization could also advance the zippering process, we induced expression of Tfap2c/Tead4/RhoA-Q63L either in the whole embryo or in half of the embryo to trigger 4-cell stage polarization and followed subsequent development by time-lapse microscopy. The induced premature polarization resulted in zippered domains associated with the tight junction protein ZO-1, not at the 16-cell but at the 8-cell stage (Fig.S8B-F). Thus, embryo polarization is sufficient to advance the subsequent step of embryogenesis leading to blastocyst formation.

As polarization in the mouse embryo is followed by cell fate specification, we determined whether overexpressing Tfap2c/Tead4/RhoA-Q63L to induce polarization at the 4-cell stage would advance differentiation of cells inheriting an apical domain into TE. Premature polarization induced premature expression of the TE transcription factors Cdx2 and Gata3 in a cell-autonomous manner (Fig.S8G-K; Movie S9-10). Thus, the combined activities of Tfap2c, Tead4, and RhoA-Q63L are sufficient to advance the timing not only of polarization but also the differentiation program.

Tfap2c/Tead4 are required for apical protein centralization

To define the relative roles of RhoA, Tfap2c, and Tead4 in driving polarization, we visualized events leading to apical domain formation in living embryos expressing LifeAct-GFP and Ezrin-RFP from the mid- to late- 8 cell-stages. During apical protein polarization, Ezrin-RFP first became concentrated at the center of the cell-contact free surface to form an apical patch concomitant with a local reduction of actin. We refer to this stage as “centralization” (Fig.4A-B; Movie S11). This apical patch of Ezrin-GFP expanded and actin became concentrated in a ring around it. We refer to this phase as “expansion” (Fig.4A,C; Movie S11). Downregulation of Tfap2c and Tead4 diminished the initial centralization of Ezrin-RFP (Fig.4D; Fig.2G), implying that centralization is required for apical domain formation.

Tfap2c/Tead4 control polarized growth of apical protein clusters

Imaging of apical domain centralization in mid- to late-8 cell stage embryos with higher temporal-spatial resolution (Movie S12) revealed Ezrin formed clusters that co-

localized with actin clusters when the embryo had just compacted but not yet polarized (Fig.4E, J). As polarization progressed, the Ezrin clusters grew; those clusters more distant grew faster than those near cell-cell contacts resulting in Ezrin enrichment towards the middle of cell-contact free surface (Fig.4E-F). The amount of membrane-associated Ezrin increased as the Ezrin clusters grew (Fig.4G) suggesting cluster growth is driven by Ezrin's recruitment to the membrane.

Overexpression of Tfap2c/Tead4 led to an increase in membrane enrichment of Ezrin and precocious growth of both Ezrin and actin clusters at the late 4-cell stage (Fig.4H-I, L-N). By contrast, Tfap2c/Tead4 depletion decreased Ezrin's membrane enrichment and prevented growth of Ezrin and actin clusters at the mid 8-cell stage (Fig.4J-N). Together, this suggests that Tfap2c/Tead4 are required for the growth of actin and apical protein clusters, recruitment of apical protein to the membrane, and centralization of apical protein.

Tfap2c/Tead4 regulate actin dynamics to promote apical protein cluster growth

Since our results suggested that Tfap2c/Tead4 could regulate actin dynamics to direct the growth of apical protein clusters, we next examined the cortical movements generated by the contractile actomyosin network during apical domain formation (*23*) (Movie S13). We first tested whether such cortical movements can drive asymmetric growth of apical protein clusters by tracking LifeAct and Ezrin clusters using Particle Image Velocimetry (PIV) (Movie S14; Methods). PIV did not detect any obvious movement toward the center of the cell-contact free surface (Fig.S9A-B) in contrast to actin flows of post-mitotic cells (*22*)(Fig.S9C). In accord, we found that inhibiting actin flows with Blebbistatin failed to prevent asymmetric Ezrin cluster growth (Fig.S9D-G; Movie S15). Thus, asymmetric clustering of Ezrin is not driven by the cortical flow mediated by actomyosin contractility.

Time-lapse observations revealed that Ezrin cluster growth occurred during the merging and splitting of actin clusters and was unimpeded by Blebbistatin (Fig.5A), suggesting that cortical actin remodeling may allow Ezrin's recruitment to growing clusters. In accord, perturbing actin de-polymerization in 8-cell embryos with Jasplakinolide (JASP) prevented apical domain formation (Fig.S9H,K). Moreover, when we inhibited the Arp2/3 complex with CK666 to prevent actin nucleation, Ezrin

cluster growth (Fig.5B-C) and apical domain formation (Fig.S9I,K) were also blocked. By contrast, treatment of embryos with a Formin inhibitor (SMiFH2) did not affect apical domain formation (Fig.S9J, L). These observations indicate actin remodeling is required for Ezrin clustering and apical domain formation. We also found that CK666 abolished apical protein polarization induced by Tfap2c/Tead4 overexpression in 4-cell embryos (Fig.5D-E). Thus, Tfap2c/Tead4-dependent regulation of actin dynamics is required for the growth of Ezrin clusters and apical protein formation.

Tfap2c/Tead4 control expression of actin regulators

To view events downstream of Tfap2c/Tead4, we carried out RNA-sequencing of 8-cell stage embryos depleted of Tfap2c and/or Tead4. For each group of embryos (control *GFP* RNAi, *Tfap2c* RNAi, *Tead4* RNAi, *Tfap2c*/*Tead4* co-RNAi), two biological replicates were collected with 10 embryos per sample and experiments performed on two strains to eliminate genetic background effects (Fig.5F, Methods). The effect of Tfap2c and Tead4 depletion was highly reproducible between biological replicates and between genetic backgrounds (Fig.S10A). Depletion of Tfap2c led to the downregulation of 749 or 929 genes (with a 2-fold differential cut-off) depending on the strain, whereas Tead4 depletion led to downregulation of 242 or 314 genes (Fig. S10B-C). Their co-depletion led to an additional 135 or 95 genes being downregulated compared to single knockdown embryos, depending on the strain (Fig.S10B-C).

A significant proportion of downregulated genes in double-knockdown embryos had actin polymerization functions (Fig.5G; Table S3). These included known actin regulators for apical domain formation, such as Cdc42 effector protein family members (Borg)(*24*), and other actin regulators, whose functions have not been explored in the mouse embryo including the Arp2/3 complex component Arpc1b, the Tropomyosin protein Tpm4, Marcks and Marcksl1 proteins, and the FREM family member Ebp4.1l5. Expression of these actin regulators becomes upregulated between the 2-cell and 8-cell stages and correlates with the size increase of actin clusters during polarization (Fig.5G). Depletion of Tfap2c and Tead4 eliminated expression of actin regulators and accordingly led to a decreased actin cluster size (Fig.4H,J-M; Fig.5G).

To test whether these actin regulators participate in apical domain formation, we depleted *Arpc1b*, *Tpm4*, *Marcksl1,* or *Ebp4.1l5* individually from 2-cell embryos and

determined the apical domain formation efficiency at the late 8-cell stage (Fig.5H-J; Fig.S11A-D). In accord with the effects of CK666, depletion of Arpc1b led to defective apical domain formation (Fig.5H-J) in natural 8-cell embryos and prevented Tfap2c/Tead4 induced apical protein polarization at the 4-cell stage (Fig.5K-L). Together, these results suggest Tfap2c and Tead4 control embryo polarization by activating expression of actin regulatory proteins.

RhoA signaling reorganizes the actin network during polarization

Knowing that not only Tfap2c/Tead4, but also RhoA-Q63L were required for apical protein clustering and apical domain formation in 4-cell embryos, we wished to determine how excess RhoA activity (by overexpressing RhoA-Q63L) or reduced RhoA activity (by treatment with RhoA inhibitor C3-transferase) at the mid 8-cell stage would affect Ezrin's membrane distribution (Fig.S12A). Overexpression of RhoA-Q63L eliminated actin and Ezrin cluster formation resulting in the homogeneous distribution of actin and Ezrin on the membrane (Fig.S12B-C). By contrast, C3-transferase treatment resulted in the ectopic clustering of actin and Ezrin on the cell membrane (Fig.S12D-E) reminiscent of 4-cell embryos overexpressing Tfap2c/Tead4 but lacking RhoA activity (Fig.3B; Fig.S7G,H). Thus, RhoA signaling is required to reorganize the actin network in the embryo and thereby the clustering of apical proteins induced by Tfap2c/Tead4.

Positive feedback and lateral mobility govern apical domain formation

To gain biophysical understanding of how Tfap2c/Tead4/RhoA regulate the timing and pattern of apical domain formation, we measured the growth of Ezrin cluster size during apical protein centralization and found it increases exponentially (Fig.4F), suggesting involvement of a positive feedback mechanism. To gain understanding of this mechanism, we tagged Ezrin with green to red photo-activatable Dendra2 fluorescent protein to track Dendra2-Ezrin movement after blue light conversion. RFP signal dynamically dissipated within seconds when Dendra2 was photo-converted at the mid 8-cell stage either within or outside the nascent apical domain, suggesting rapid Ezrin membrane turnover (Fig.6A-D). Irrespective of the site of photo-conversion, Ezrin-Dendra2 relocated to the nascent domain in proportion to the concentration of Ezrin in this area, indicating positive feedback of Ezrin on its own

accumulation. This accords with previous measurements of cooperative recruitment of Ezrin to PIP2 membranes (*25, 26*).

To determine whether Ezrin dynamics can account for apical protein centralization, we constructed a model (Methods) based on four empirically grounded assumptions (Fig. 6E): 1) a cooperative increase in Ezrin binding rate (k_{on}) with increasing Ezrin concentration saturating above a critical concentration (E_{crit}) suggested by the positive feedback above (Fig. 6B,D) and known cooperative binding of Ezrin to membranes (*25, 26*); 2) a limit to Ezrin membrane loading by the finite pool of PIP2 (P_{tot}) based on co-localization of Ezrin with PIP2 in the apical domain (Fig. S12F) and prevention of apical domain formation by reduced PIP2 (*21*); 3) lateral motility of Ezrin along the membrane as observed (Fig. 6A-D; Fig. S12G), and that can be modelled as effective diffusion with diffusivity (D_E); 4) dissociation of Ezrin at a uniform rate from the membrane (k_{off}) (Fig. 6E).

We simulated Ezrin dynamics in one dimension and estimated parameter values for simulations best fitting our experimental measurements (Methods, Supplementary Modeling). Our simulations reproduced the dynamic changes of Ezrin distribution during centralization *in vivo* (Fig.6F). The model also recapitulated the ability of single cells to form centralized Ezrin domain in the absence of cell-cell contacts (Fig.S12H, Methods) and the ability of cell-cell contacts to constrain apical Ezrin to the center of cell-contact free surface (Fig.S12I). Thus, experimental observations and computational simulation together reveal positive feedback, lateral mobility, and competition for limiting PIP2 are sufficient to explain apical protein centralization step.

Tfap2c/Tead4/RhoA control cooperative recruitment and lateral mobility of apical proteins

Our model predicts that elevating the saturation threshold (E_{crit}) for cooperative recruitment of Ezrin would change the steady-state distribution of membrane-bound Ezrin, resulting in a narrowed peak resembling the Tfap2c/Tead4 overexpression phenotype (Fig.6G, Supplementary Modeling). This suggests Tfap2c/Tead4 regulates the kinetics of the cooperative Ezrin recruitment. To test this, we computed the rate of change in membrane-bound Ezrin concentration ($\Delta E/\Delta T$) as a function of the Ezrin concentration during apical centralization, for both control and Tfpa2c/Tead4

overexpressing embryos (Fig.S12J). This revealed that when the Ezrin concentration falls below a threshold value, local Ezrin subsequently decreases but, when the local concentration exceeds this value, more Ezrin gets recruited to the membrane (Fig. S12J).

Myosin motor activity within the actin cortex can affect the lateral mobility of membrane proteins that can negatively regulate the formation of membrane clusters (*27*) suggesting that RhoA might regulate the lateral mobility of Ezrin. To test this, we quantified the "spread" of photo-converted signal (Methods) and compared the difference between control and RhoA-Q63L overexpressing cells (Fig.S12K). Elevating RhoA activity increased the spreading effect of photo-converted Ezrin on the membrane, suggesting that RhoA positively regulates the lateral mobility of Ezrin (Fig. S12K). In accord, our simulations predict that increasing lateral mobility leads to homogeneously distributed Ezrin (Fig.6G) and that insufficient lateral mobility results in multiple peaks of apical protein (Fig.S12L). These predictions are concordant with the phenotypes resulting from overexpression of RhoA-Q63L and depletion of RhoA in the 8-cell embryo (Fig.S12B-E).

Our model suggests that lateral mobility and the cooperative recruitment threshold have opposing effects on the shape of the apical patch (Fig.6H;Fig.S12M). Specifically, normal apical domain will form only when both processes are activated at an appropriate level. This prediction provides a qualitative explanation for the concurrent requirements for Tfap2c/Tead4 and RhoA signaling in regulating apical domain formation (Fig.3B; Fig.6I).

Discussion

The importance of the first appearance of apical-basal cell polarity in mammalian development is evident from its requirement to trigger the first cell fate diversification event. Here, we show that zygotic expression of Tfap2c and Tead4 is a prerequisite for such polarization. We have been able to induce precocious embryo polarization and thereby advance subsequent embryogenesis by driving the ectopic expression of Tfap2c/Tead4 and activated Rho GTPase. Our findings help account for the temporal relationship between zygotic genome activation and the establishment of embryo polarization across multiple mammalian species (*11, 12*).

Embryo polarization at the 8-cell stage has been viewed as a model for epithelial polarization. However, formation of the apical domain is distinct from many other cell types as it can occur in the absence of external cues such as the extra-cellular matrix or cell adhesion. The mechanisms behind such unique spontaneous symmetry breaking properties have remained elusive. Here we show the initial step for symmetry breaking is the centralization of apical proteins through their two types of behavior on the membrane: actin-mediated cooperative recruitment and lateral mobility. These two processes act as opposing forces to regulate the shape of the apical domain; a cooperative recruitment mechanism enables symmetry breaking and concentration of the apical proteins whereas lateral mobility allows apical proteins to diffuse, thereby establishing a crescent-shape patch (Fig.6G-H; Fig.S12M). The balanced activity between the two processes ensures the proper shape of the apical domain because an excessive cooperative recruitment force would lead to small and often multiple domains, whereas excessive lateral mobility would lead to the uniform distribution of apical proteins and thereby inhibit symmetry breaking (Fig.6G; Fig.S12L).

Our results suggest that cooperative recruitment is regulated by actin remodeling controlled by Tfap2c and Tead4. Although the detailed mechanism is beyond the scope of this work, it is possible that Ezrin is preferentially recruited to the actin structure promoted by the Arp2/3 complex in a process similar to protein condensation (*28*). In such a case, the density of the branched actin network would positively impact on the saturation level of Ezrin in the cooperative recruitment process. It has been observed *in vitro* that the actin clusters formed by Arp2/3 activity are degraded by high levels of cortical myosin (*29*), which could explain the opposing effects between Tfap2c/Tead4 and RhoA in regulating the apical protein clustering and accordingly the apical domain shape.

The regulatory regime we describe is based on the behavior of Ezrin and it is likely to apply to other apical proteins such as the Par complex, whose polarization dynamics are highly similar and also require the actin network and membrane binding, the key conditions of the process we describe (*21*). Our work illustrates how the embryo establishes cell polarization at a specific developmental stage under the regulation of stage-dependent pathways. Our results also provide a biophysical explanation for how

polarization is established, indicating that positive feedback combined with lateral mobility are sufficient to drive this self-organization process. These results therefore provide insight into both the timing and mechanism of the establishment of *de novo* polarization in the mouse embryo, the critical event for the first cell fate specification.

References:

1. E. Korotkevich et al., The Apical Domain Is Required and Sufficient for the First Lineage Segregation in the Mouse Embryo. Developmental cell 40, 235-247 e237 (2017).

2. M. H. Johnson, C. A. Ziomek, The foundation of two distinct cell lineages within the mouse morula. Cell 24, 71-80 (1981).

3. M. H. Johnson, C. A. Ziomek, Induction of polarity in mouse 8-cell blastomeres: specificity, geometry, and stability. The Journal of cell biology 91, 303-308 (1981).

4. T. P. Fleming, P. M. Cannon, S. J. Pickering, The cytoskeleton, endocytosis and cell polarity in the mouse preimplantation embryo. Developmental biology 113, 406-419 (1986).

5. S. Louvet, J. Aghion, A. Santa-Maria, P. Mangeat, B. Maro, Ezrin becomes restricted to outer cells following asymmetrical division in the preimplantation mouse embryo. Developmental biology 177, 568-579 (1996).

6. B. Plusa et al., Downregulation of Par3 and aPKC function directs cells towards the ICM in the preimplantation mouse embryo. Journal of cell science 118, 505-515 (2005).

7. N. Nishioka et al., The Hippo signaling pathway components Lats and Yap pattern Tead4 activity to distinguish mouse trophectoderm from inner cell mass. Developmental cell 16, 398-410 (2009).

8. A. Ralston et al., Gata3 regulates trophoblast development downstream of Tead4 and in parallel to Cdx2. Development 137, 395-403 (2010).

9. M. H. Johnson, J. McConnell, J. Van Blerkom, Programmed development in the mouse embryo. Journal of embryology and experimental morphology 83 Suppl, 197-231 (1984).

10. S. A. Morris, Y. Guo, M. Zernicka-Goetz, Developmental plasticity is bound by pluripotency and the Fgf and Wnt signaling pathways. Cell reports 2, 756-765 (2012).

11. H. Koyama, H. Suzuki, X. Yang, S. Jiang, R. H. Foote, Analysis of polarity of bovine and rabbit embryos by scanning electron microscopy. Biology of reproduction 50, 163-170 (1994).

12. G. Nikas, A. Ao, R. M. Winston, A. H. Handyside, Compaction and surface polarity in the human embryo in vitro. Biology of reproduction 55, 32-37 (1996).

13. T. Hamatani, M. G. Carter, A. A. Sharov, M. S. Ko, Dynamics of global gene expression changes during mouse preimplantation development. Developmental cell 6, 117-131 (2004).

14. O. Padovan-Merhar et al., Single mammalian cells compensate for differences in cellular volume and DNA copy number through independent global transcriptional mechanisms. Molecular cell 58, 339-352 (2015).

15. M. Bao, J. Xie, A. Piruska, W. T. S. Huck, 3D microniches reveal the importance of cell size and shape. Nature communications 8, 1962 (2017).

16. M. Zernicka-Goetz, Fertile offspring derived from mammalian eggs lacking either animal or vegetal poles. Development 125, 4803-4808 (1998).

17. F. Wang et al., RNAscope: a novel in situ RNA analysis platform for formalin-fixed, paraffin-embedded tissues. J Mol Diagn 14, 22-29 (2012).

18. Q. Deng, D. Ramskold, B. Reinius, R. Sandberg, Single-cell RNA-seq reveals dynamic, random monoallelic gene expression in mammalian cells. Science 343, 193-196 (2014).

19. J. Wu et al., The landscape of accessible chromatin in mammalian preimplantation embryos. Nature 534, 652-657 (2016).

20. Y. Hirate et al., Par-aPKC-dependent and -independent mechanisms cooperatively control cell polarity, Hippo signaling, and cell positioning in 16-cell stage mouse embryos. Development, growth & differentiation 57, 544-556 (2015).

21. M. Zhu, C. Y. Leung, M. N. Shahbazi, M. Zernicka-Goetz, Actomyosin polarisation through PLC-PKC triggers symmetry breaking of the mouse embryo. Nature communications 8, 921 (2017).

22. J. Zenker et al., Expanding Actin Rings Zipper the Mouse Embryo for Blastocyst Formation. Cell 173, 776-791 e717 (2018).

23. J. L. Maitre, R. Niwayama, H. Turlier, F. Nedelec, T. Hiiragi, Pulsatile cell-autonomous contractility drives compaction in the mouse embryo. Nature cell biology 17, 849-855 (2015).

24. Q. P. Vong et al., A role for borg5 during trophectoderm differentiation. Stem cells 28, 1030-1038 (2010).

25. A. Herrig et al., Cooperative adsorption of ezrin on PIP2-containing membranes. Biochemistry 45, 13025-13034 (2006).

26. J. J. Jayasundar et al., Open conformation of ezrin bound to phosphatidylinositol 4,5-bisphosphate and to F-actin revealed by neutron scattering. The Journal of biological chemistry 287, 37119-37133 (2012).

27. B. D. Slaughter et al., Non-uniform membrane diffusion enables steady-state cell polarization via vesicular trafficking. Nature communications 4, 1380 (2013).

28. S. F. Banani, H. O. Lee, A. A. Hyman, M. K. Rosen, Biomolecular condensates: organizers of cellular biochemistry. Nature reviews. Molecular cell biology 18, 285-298 (2017).

29. K. A. Ganzinger, S. K. Vogel, J. Mücksch, P. Blumhardt, P. Schwille, others, Myosin-ii activity generates a dynamic steady state with continuous actin turnover in a minimal actin cortex. Journal of Cell Science. 132 (2019).

30. S. Efrat, R. Kaempfer, Control of biologically active interleukin 2 messenger rna formation in induced human lymphocytes. *Proceedings of the National Academy of Sciences*. **81**, 2601–2605 (1984).

31. O. Bensaude, Inhibiting eukaryotic transcription. Which compound to choose? How to evaluate its activity? Which compound to choose? How to evaluate its activity? *Transcription*. **2**, 103–108 (2011).

32. S. Vispé, L. DeVries, L. Créancier, J. Besse, S. Bréand, D. J. Hobson, J. Q. Svejstrup, J.-P. Annereau, D. Cussac, C. Dumontet, others, Triptolide is an inhibitor

of rna polymerase i and ii–dependent transcription leading predominantly to down-regulation of short-lived mRNA. *Molecular cancer therapeutics*. **8**, 2780–2790 (2009).

33. L. Clayton, A. Hall, M. Johnson, A role for rho-like gtpases in the polarisation of mouse eight-cell blastomeres. *Developmental biology*. **205**, 322–331 (1999).

34. B. Hetrick, M. S. Han, L. A. Helgeson, B. J. Nolen, Small molecules ck-666 and ck-869 inhibit actin-related protein 2/3 complex by blocking an activating conformational change. *Chemistry & biology*. **20**, 701–712 (2013).

35. A. Holzinger, in *Cytoskeleton methods and protocols* (Springer, 2009), pp. 71–87.

36. S. J. Graham, K. B. Wicher, A. Jedrusik, G. Guo, W. Herath, P. Robson, M. Zernicka-Goetz, BMP signalling regulates the pre-implantation development of extra-embryonic cell lineages in the mouse embryo. *Nature communications*. **5**, 1–11 (2014).

37. M. Zernicka-Goetz, J. Pines, S. H. McLean, J. Dixon, K. Siemering, J. Haseloff, M. Evans, Following cell fate in the living mouse embryo. *Development*. **124**, 1133–1137 (1997).

38. T. Horn, M. Boutros, E-rnai: A web application for the multi-species design of rnai reagents—2010 update. *Nucleic acids research*. **38**, W332–W339 (2010).

39. J. Schindelin, I. Arganda-Carreras, E. Frise, V. Kaynig, M. Longair, T. Pietzsch, S. Preibisch, C. Rueden, S. Saalfeld, B. Schmid, others, Fiji: An open-source platform for biological-image analysis. *Nature methods*. **9**, 676–682 (2012).

40. S. Picelli, O. R. Faridani, Å. K. Björklund, G. Winberg, S. Sagasser, R. Sandberg, Full-length rna-seq from single cells using smart-seq2. *Nature protocols*. **9**, 171–181 (2014).

41. B. R. Brückner, A. Pietuch, S. Nehls, J. Rother, A. Janshoff, Ezrin is a major regulator of membrane tension in epithelial cells. *Scientific Reports*. **5**, 14700 (2015).

42. O. Turunen, T. Wahlström, A. Vaheri, Ezrin has a COOH-terminal actin-binding site that is conserved in the ezrin protein family. *The Journal of Cell Biology*. **126**, 1445–1453 (1994).

43. R. Gary, A. Bretscher, Ezrin self-association involves binding of an n-terminal domain to a normally masked c-terminal domain that includes the f-actin binding site. *Molecular Biology of the Cell*. **6**, 1061–1075 (1995).

44. V. Niggli, C. Andréoli, C. Roy, P. Mangeat, Identification of a phosphatidylinositol-4, 5-bisphosphate-binding domain in the n-terminal region of ezrin. *Federation of European Biochemical Societies Letters*. **376**, 172–176 (1995).

45. B. T. Fievet, A. Gautreau, C. Roy, L. Del Maestro, P. Mangeat, D. Louvard, M. Arpin, Phosphoinositide binding and phosphorylation act sequentially in the activation mechanism of ezrin. *The Journal of Cell Biology*. **164**, 653–659 (2004).

46. M. Fritzsche, R. Thorogate, G. Charras, Quantitative analysis of ezrin turnover dynamics in the actin cortex. *Biophysical Journal*. **106**, 343–353 (2014).

47. J.-J. Hao, Y. Liu, M. Kruhlak, K. E. Debell, B. L. Rellahan, S. Shaw, Phospholipase c–mediated hydrolysis of PIP2 releases ERM proteins from lymphocyte membrane. *Journal of Cell Biology*. **184**, 451–462 (2009).

48. Y. Mori, A. Jilkine, L. Edelstein-Keshet, Wave-pinning and cell polarity from a bistable reaction-diffusion system. *Biophysical Journal*. **94**, 3684–3697 (2008).

49. J.-G. Chiou, S. A. Ramirez, T. C. Elston, T. P. Witelski, D. G. Schaeffer, D. J. Lew, Principles that govern competition or co-existence in rho-gtpase driven polarization. *PLoS Computational Biology*. **14**, e1006095 (2018).

50. N. W. Goehring, P. K. Trong, J. S. Bois, D. Chowdhury, E. M. Nicola, A. A. Hyman, S. W. Grill, Polarization of par proteins by advective triggering of a pattern-forming system. *Science*. **334**, 1137–1141 (2011).

51. S. Zonies, F. Motegi, Y. Hao, G. Seydoux, Symmetry breaking and polarization of the c. Elegans zygote by the polarity protein par-2. *Development*. **137**, 1669–1677 (2010).

52. P. K. Trong, E. M. Nicola, N. W. Goehring, K. V. Kumar, S. W. Grill, Parameter-space topology of models for cell polarity. *New Journal of Physics*. **16**, 065009 (2014).

53. P. Gross, K. V. Kumar, N. W. Goehring, J. S. Bois, C. Hoege, F. Jülicher, S. W. Grill, Guiding self-organized pattern formation in cell polarity establishment. *Nature Physics*. **15**, 293–300 (2019).

54. A. B. Goryachev, A. V. Pokhilko, Dynamics of Cdc42 network embodies a turing-type mechanism of yeast cell polarity. *FEBS letters*. **582**, 1437–1443 (2008).

55. A. B. Goryachev, M. Leda, Many roads to symmetry breaking: Molecular mechanisms and theoretical models of yeast cell polarity. *Molecular Biology of the Cell*. **28**, 370–380 (2017).

56. M. Otsuji, S. Ishihara, K. Kaibuchi, A. Mochizuki, S. Kuroda, others, A mass conserved reaction–diffusion system captures properties of cell polarity. *PLoS Comput Biol*. **3**, e108 (2007).

57. S. J. Altschuler, S. B. Angenent, Y. Wang, L. F. Wu, On the spontaneous emergence of cell polarity. *Nature*. **454**, 886–889 (2008).

58. J. Cornwall-Scoones, D. S. Banerjee, S. Banerjee, Size-regulated symmetry breaking in reaction-diffusion models of developmental transitions. *Cells*. **9**, 1646 (2020).

59. S. A. Menchón, A. Gärtner, P. Román, C. G. Dotti, Neuronal (Bi)polarity as a self-organized process enhanced by growing membrane. *PLoS One*. **6**, e24190 (2011).

60. C. A. Parent, P. N. Devreotes, A cell's sense of direction. *Science*. **284**, 765–770 (1999).

61. P. Devreotes, A. R. Horwitz, Signaling networks that regulate cell migration. *Cold Spring Harbor perspectives in biology*. **7**, a005959 (2015).

62. Y. Xiong, C.-H. Huang, P. A. Iglesias, P. N. Devreotes, Cells navigate with a local-excitation, global-inhibition-biased excitable network. *Proceedings of the National Academy of Sciences*. **107**, 17079–17086 (2010).

63. H. Meinhardt, A. Gierer, Pattern formation by local self-activation and lateral inhibition. *Bioessays*. **22**, 753–760 (2000).

64. S. MacNamara, G. Strang, in *Splitting methods in communication, imaging, science, and engineering* (Springer, 2016), pp. 95–114.

65. F. Etoc, J. Metzger, A. Ruzo, C. Kirst, A. Yoney, M. Z. Ozair, A. H. Brivanlou, E. D. Siggia, A balance between secreted inhibitors and edge sensing controls gastruloid self-organization. *Developmental Cell*. **39**, 302–315 (2016).

66. N. W. Goehring, D. Chowdhury, A. A. Hyman, S. W. Grill, FRAP analysis of membrane-associated proteins: Lateral diffusion and membrane-cytoplasmic exchange. *Biophysical Journal*. **99**, 2443–2452 (2010).

67. D. S. Banerjee, S. Banerjee, Size regulation of multiple organelles competing for a shared subunit pool. *bioRxiv (pre-print)* (2020).

68. R. Geßele, J. Halatek, L. Würthner, E. Frey, Geometric cues stabilise long-axis polarisation of par protein patterns in c. Elegans. *Nature Communications*. **11**, 1–12 (2020).

69. Q. Chen, J. Shi, Y. Tao, M. Zernicka-Goetz, Tracing the origin of heterogeneity and symmetry breaking in the early mammalian embryo. *Nature Communications*. **9**, 1–11 (2018).

Acknowledgement: We are grateful to E. Munro, D. Glover, A. Andersen, M. Shahbazi for helpful discussion; S. Shadkhoo for comments on the model; S. Malas for the Gata3-GFP transgenic line. Some of the computations were conducted on the Caltech High Performance Cluster, supported by the Gordon and Betty Moore Foundation grant. This work was supported by grants from Wellcome Trust (098287/Z/12/Z), ERC (669198), Leverhulme Trust (RPG-2018-085), Open Philanthropy/Silicon Valley, Weston Havens Foundations and NIH R01 HD100456-01A1 to M.Z.G. Packard Foundation, Heritage Medical Research Institute, NIH U01CA244109 to M.T. The National Key R&D Program of China Grant 2017YFA0102802 and 2019YFA0110001 to J.N. **Author contributions**: Conceptualization: M.Z and M.Z.G; Investigation: M.Z., J.C.S., P.W., C.H; Writing: M.Z and M.Z.G; Supervision: M.Z.G, N.J. **Declaration of Interests**: The authors declare no competing interests. **Data and materials availability:** All raw data are available

upon request from corresponding author. The RNA-sequencing data has been deposited on GEO database (accession number: GSE124755); the code for computation simulation has been deposited on https://jakesorel.github.io/Apical_Domain_2020/.

Summary of the method

This research followed regulations of the Animals (Scientific Procedures) Act 1986 - Amendment Regulations 2012 - reviewed by the University of Cambridge Animal Welfare and Ethical Review. Embryos were collected from superovulated F1 females (C57Bl6xCBA) crossed with F1 males. For embryo culture and inhibitor treatment, embryos were recovered at the zygote or 2-cell stage in M2 medium and transferred to KSOM medium for long-term culture. The inhibitors, or the same amount of vehicles (for control condition), were applied to the culture. The microinjection procedure, immunostaining, static imaging and image processing, and real-time qPCR were carried out as previously described (*21*). For photo-conversion experiment, region of interest (ROI) covered a rectangular region of length roughly 5μm and width roughly 2μm on the membrane of cells expressing Ezrin-Dendra2, using the mid-plane of the blastomeres as a reference. The ROI was illuminated at 405nm for 5s, after which converted proteins were imaged with a 568nm laser and at an emission wavelength between 580-620nm, in every 2s/frame for 5min. The converted scanning speed is 200Hz, and the normal scanning speed is 700Hz. For all imaging settings, the images have been recorded using the 1024x1024 pixel format. Particle Image Velocimetry (PIV) analysis was performed using PIVlab MATLAB algorithm (pivlab.blogspot.de). For statistics, the sample distribution as well as statistic tests were performed using Prism software (http://www.graphpad.com).

Details of the materials and methods, as well as the details for RNA-sequencing and modeling methods can be found in the supplementary materials.

Figure Legends

Figure 1. The dependency of polarization on nascent transcripts. (A) Scheme indicating inhibitor treatments. (**B**) DMSO (control)- or DRB-treated 8-16-cell embryos analyze F-actin, Pard6 and DNA. (**C**) Polarized cell number in DMSO (control) or DRB-

treated embryos. ****p<0.0001, Mann-Whitney U test. N=2 experiments. (**D**) Apical enrichment of Pard6 (Methods) in 8-16-cell stage cells treated with DMSO (control) or DRB. ****p<0.0001. Mann-Whitney U test. (**E**) Scheme of the hypothesis: newly synthesized factors important for polarization accumulate up to a point upon which polarization is induced at the 8-cell stage. Decreasing the cell size would elevate the concentration of such factors leading to an advance in polarization timing. (**F**) Scheme showing blastomere resection procedure. (**G,H**) Time-lapse of control or smaller sister blastomeres from experiment in **F**. Arrows indicate the apical domain. Yellow squares indicate the magnified regions (top). (**I,J**) Polarization time difference (Methods) between smaller and control sister blastomeres from **F** or Fig. S2F, each bar represents one comparison. Smaller cells polarize earlier in the significant majority of cases. N=13 experiments for **I**, N=6 experiments for **J**. ****p<0.0001, one-sample t-test, hypothetical mean=0. (**K**) Polarization time difference between control and smaller DRB-treated sister cells, from experiments in Fig. S2L. Each bar represents one comparison. Pulsed transcription inhibition prevents the early polarization of smaller cells. N=3 experiments. ns, not significant, one-sample t-test, hypothetical mean =0. Arrows indicate the apical domain. Scale bars, 15μm.

Figure 2. Zygotic expression of Tfap2c and Tead4 is essential for polarization. (**A-D**) Time-lapse of Ezrin-RFP localization in embryos with or without Tfap2c and/or Tead4. Tfap2c and Tead4 co-depletion causes polarization failure until the 16-cell stage. Arrows indicate apical domain. (**E,F**) Polarized cell number in different conditions and stages. Each dot represents an embryo. dsTT: dsTfap2c+dsTead4. *p=0.0306; ***p=0.0006; ****p<0.0001. Kruskal-Wallis test for **E**, one-way ANOVA test for **F**. (**G**) F-actin, Pard6, and Ezrin localization in late 8-cell stage embryos injected with dsGFP (control) or dsTT. (**H**) Quantification of Ezrin apical enrichment. ****p<0.0001, Student's t-test. (**I**) CRISPR-Cas9 strategy to deplete Tfap2c and Tead4. (**J**) Tfap2c and Tead4 protein levels in wild-type (Cas9 mRNA, control); Tfap2c depleted (with Tfap2c sgRNAs); Tead4 depleted (with Tead4 sgRNAs); Tfap2c and Tead4 co-depleted (with sgRNAs targeting both Tfap2c and Tead4), Ezrin-RFP expressing embryos. (**K**) Proportions of polarized cells in different genotypes presented in **J**. Number of cells analyzed presented within each bar. ns, not significant; ****p<0.0001, Fisher's exact test. N=2 experiments. Tfap2c and Tead4 co-depletion represses apical domain formation. (**L**) Quantifications of Ezrin apical enrichment.

Each dot represents a cell. **p=0.0012, ***p=0.0007, ****p<0.0001, Kruskal-Wallis test. N=4 experiments. Scale bars, 15μm.

Figure 3. Premature expression of Tfap2c, Tead4, and activated-RhoA is sufficient to advance polarization timing. (**A**) Scheme of Tfap2c, Tead4, and RhoA-Q63L overexpression. (**B**) Ezrin-Venus dynamics in late 4-cell or 8-cell stage control cells (Ezrin-Venus only); or late 4-cell stage cells overexpressing a)Tfap2c+Tead4(TT); b)RhoA-Q63L(RhoA) or c)Tfap2c+Tead4+RhoA-Q63L(TTRhoA). Tfap2c+Tead4+RhoA-Q63L overexpression induces premature, full apical domain. In all conditions cell divisions were not affected. Short arrows indicate Ezrin-Venus enrichment at the cell-contact free surface. Long arrows indicate apical domain expansion. Squares indicate the magnified regions. (**C**) Quantification of morphologies induced by conditions in **B**. Number of cells analyzed presented within each bar. (**D**) Scheme of Tfap2c, Tead4, and RhoA-Q63L overexpression. (**E**) Representative images of embryos overexpressed with Ezrin-RFP, LifeAct-GFP mRNA only (control) or with Tfap2c, Tead4 and RhoA-Q63L mRNA at 4- or 8-cell stage. The cells overexpressed with Tfap2c, Tead4 and RhoA-Q63L polarize significantly earlier than control cells in the same embryos, or cells in the control embryos. Arrows indicate the apical domain. (**F**) Polarization time difference between cells with or without LifeAct-GFP or Tfap2c+Tead4+RhoA-Q63L overexpression in the same embryo, or in control embryos. ns, not significant; ****p<0.0001, one-sample t-test. hypothetical mean = 0. Control group: N=13 embryos ; TTRhoA group: N=19 embryos . N=2 experiments. Scale bars, 15μm.

Figure 4. Tfap2c and Tead4 regulate apical domain centralization through regulating the apical protein clustering. (**A**) LifeAct- GFP and Ezrin-RFP dynamics during polarization. Squares denote magnified regions; yellow and grey arrows indicate apical protein or actin ring movements. The apical domain forms following centralization and expansion steps. N=7 embryos, N=4 experiments. (**B,C**) Ezrin-RFP signal at the cell-contact free surface during centralization or expansion steps in **A**. Ezrin signal is normalized against average membrane signal intensity. (**D**) Ezrin-RFP distribution on cell-contact free surface at the late 8-cell stage in dsGFP (control) or dsTfap2c+dsTead4 injected cells. Numbers indicate examined cells. N=2 experiments. (**E**) Ezrin-RFP distribution during apical centralization. (**F**) Ezrin cluster

size during polarization. More than 1500 clusters were analyzed for each time-point. Data shown as mean ± S.D. N=2 experiments. (**G**) Ezrin membrane enrichment during centralization. N=4 cells from 4 embryos. Data shown as mean ± S.E.M. (**H**-**K**) Localization of LifeAct-GFP and Ezrin-RFP in embryos injected with or without Tfap2c+Tead4 mRNA at late 4-cell stage, or embryos injected with or without dsTfap2c+dsTead4 at 8-cell stage. Yellow squares indicate magnified regions (right). (**L**,**M**) Size of actin (**L**) or Ezrin (**M**) clusters in embryos shown in (**H-K**). Data shown as mean ± S.E.M. ***p<0.001, ****p<0.0001, One-way ANOVA test. Numbers indicate examined cells. More than 500 clusters were measured in each condition. (**N**) Ezrin membrane enrichment in different conditions and stages. TT, Tfap2c+Tead4 overexpression; dsTT, dsTfap2c+dsTead4 knockdown. Numbers indicate examined cells. Data presented as mean ± S.E.M. Scale bars for magnified images in **H-K**, 5μm. All other scale bars, 15μm.

Figure 5. Clustering of apical proteins is regulated by local actin dynamics. (**A**) LifeAct-GFP and Ezrin-RFP dynamics with or without Blebblstatin treatment during polarization. Arrows indicate the merging of Ezrin clusters during actin polymerization. Scale bar, 1μm. N=5 cells for each condition. N=3 experiments. Blebbistatin treatment did not prevent the clustering of actin or Ezrin proteins. (**B**) LifeAct-GFP and Ezrin-RFP localization in mid 8-cell stage embryos treated with DMSO (control) and CK666. Scale bars, 5μm. (**C**) Ezrin cluster size in cells treated with DMSO or CK666 in **B**. ****p<0.0001, Mann-Whitney U test. More than 1500 clusters were measured in each condition, N=2 experiments. (**D**) F-actin and Ezrin-RFP localization in late 4-cell embryos expressing Ezrin-RFP only, or with Tfap2c+Tead4 treated with or without CK666. (**E**) Ezrin cluster size in **D**. ****p<0.0001, Kruskal-Wallis test. More than 1100 clusters were calculated in each condition, N=2 experiments. (**F**) Experimental strategy for RNA-sequencing. (**G**) Heatmap showing the expression of selective cytoskeleton regulators downstream of Tfap2c and Tead4. (**H**) LifeAct-GFP and Ezrin-RFP localization in dsGFP or dsArpc1b injected embryos. (**I**) Polarized cell numbers in dsGFP and dsArpc1b groups. Numbers represent cell number. ***p<0.001, Fisher's exact test. (**J**) Ezrin-RFP apical enrichment in dsGFP or dsArpc1b cells. Each dot represents a cell. ***p<0.001, Student's t-test. (**K**) LifeAct-GFP and Ezrin-RFP localization in different conditions. Squares indicate magnified regions (right). (**L**) Number of cells showing apical protrusions in **K**. Scale bars, 15μm.

Figure 6. Tfap2c/Tead4/RhoA regulate apical domain formation through a positive feedback and mobility system. (**A,C**) Ezrin-Dendra2 localization during and after photoconversion. Yellow squares indicate converted region, red and green squares indicate Ezrin-high or low regions measured in **B** and **D**. (**B**,**D**) Signal intensity of converted Ezrin-Dendra2 (experimental setting shown in **A** and **C**) in Ezrin-low and Ezrin-high regions within 6 min post-conversion. Scale bars, 15μm. (**E**) Structure of the biophysical model. (**F**) Kymographs comparing *in silico* and *in vivo* polarization dynamics. Same color corresponds to the same Ezrin intensity. (**G**) Time courses of simulated Ezrin apical distribution at different regions of parameter space. Colors corresponding to the elapsed simulation time. (**H**) Phase space of polarization shape within the monopolar regime. (**I**) Summary of the results.

Figure 1

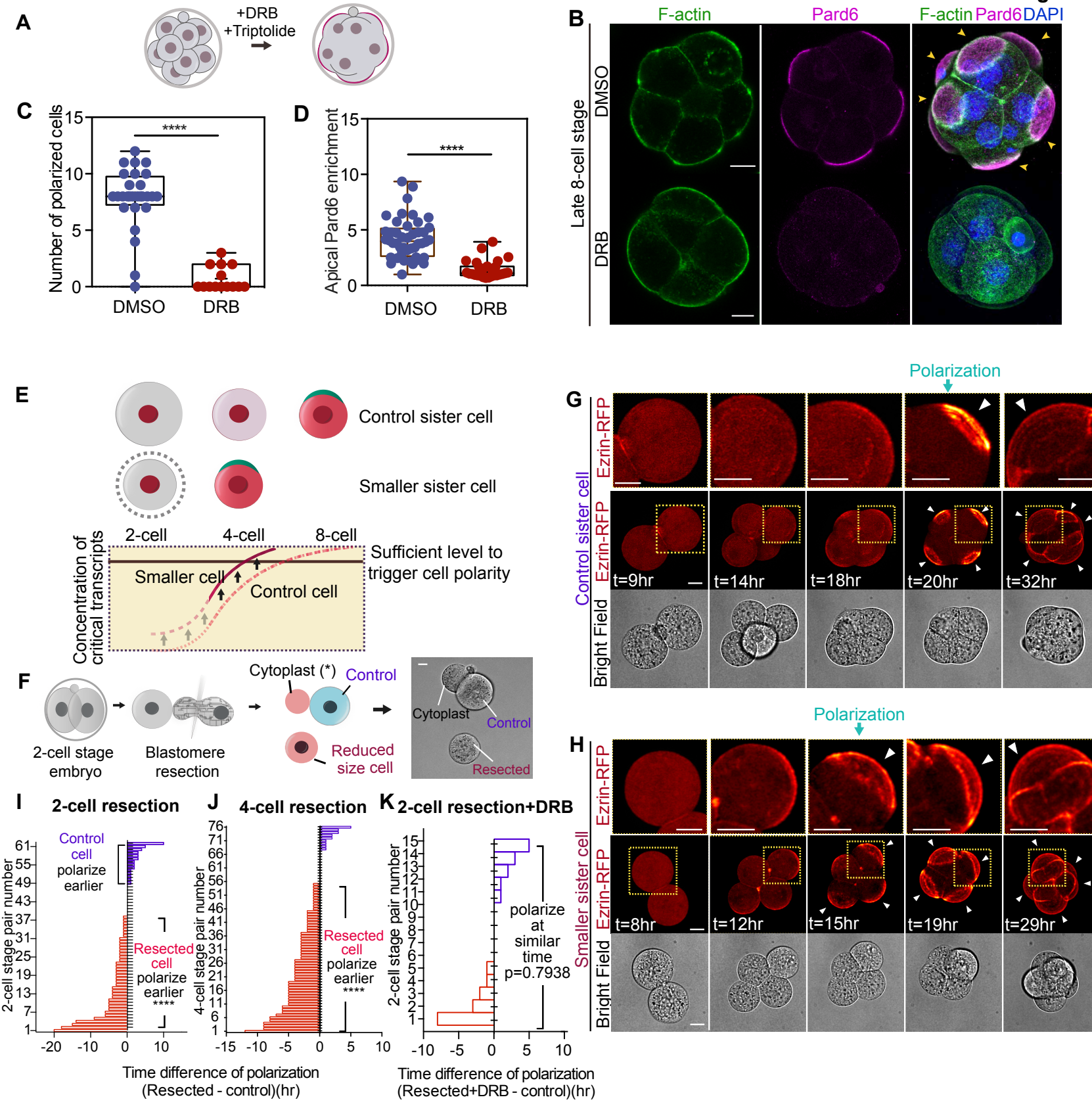
A
+DRB
+Triptolide
B
F-actin
Pard6
F-actin Pard6 DAPI
Late 8-cell stage
DMSO
DRB
C
Number of polarized cells
****
DMSO
DRB
D
Apical Pard6 enrichment
****
DMSO
DRB
E
Control sister cell
Smaller sister cell
2-cell
4-cell
8-cell
Concentration of critical transcripts
Smaller cell
Control cell
Sufficient level to trigger cell polarity
F
2-cell stage embryo
Blastomere resection
Cytoplast (*)
Control
Reduced size cell
Cytoplast
Control
Resected
G
Polarization
Ezrin-RFP
Control sister cell
Ezrin-RFP
t=9hr
t=14hr
t=18hr
t=20hr
t=32hr
Bright Field
H
Polarization
Ezrin-RFP
Smaller sister cell
Ezrin-RFP
t=8hr
t=12hr
t=15hr
t=19hr
t=29hr
Bright Field
I
2-cell resection
Control cell polarize earlier
Resected cell polarize earlier
****
2-cell stage pair number
Time difference of polarization (Resected - control)(hr)
J
4-cell resection
Resected cell polarize earlier
****
4-cell stage pair number
K
2-cell resection+DRB
polarize at similar time p=0.7938
2-cell stage pair number
Time difference of polarization (Resected+DRB - control)(hr)

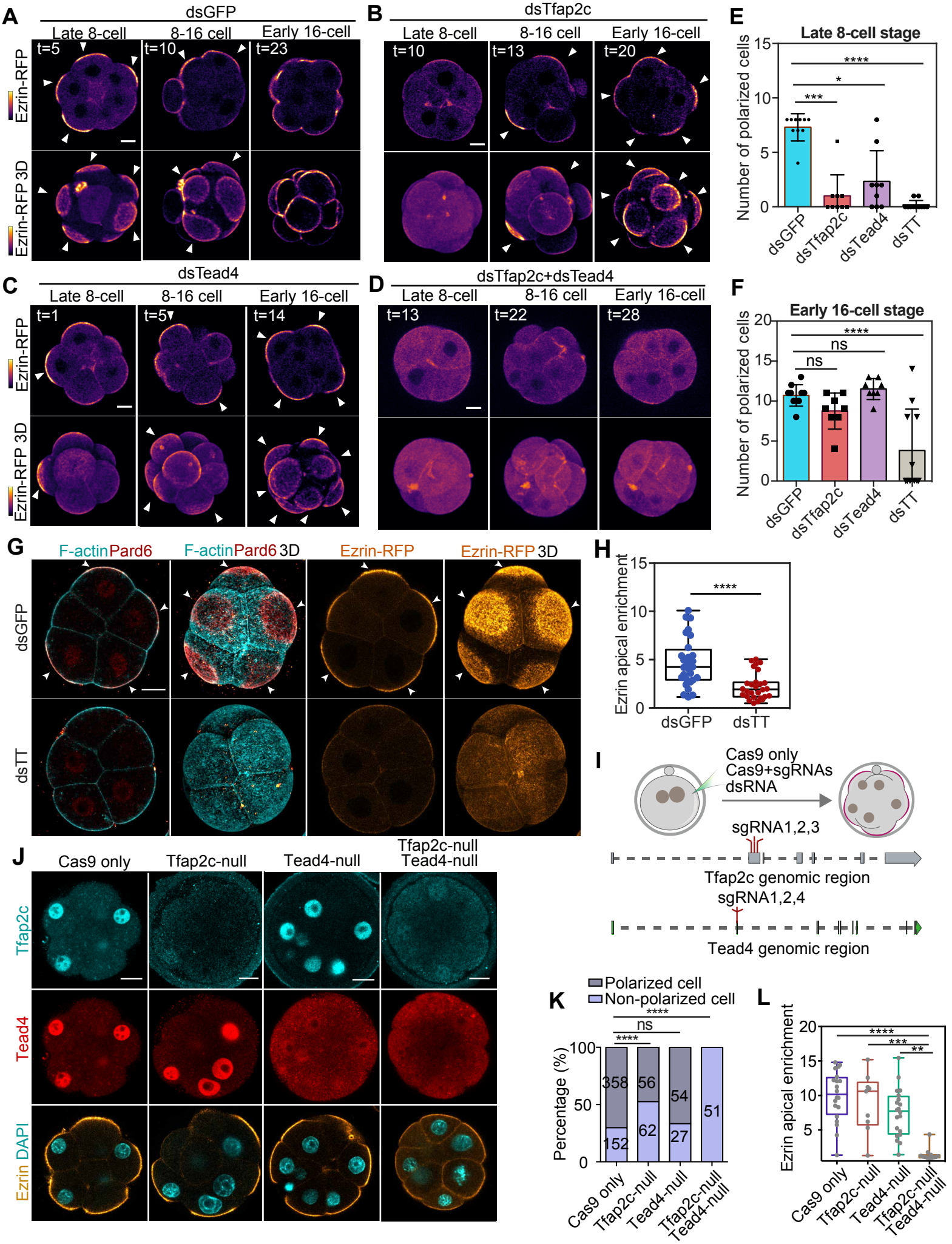
A
dsGFP
Late 8-cell
8-16 cell
Early 16-cell
t=5
t=10
t=23
Ezrin-RFP
Ezrin-RFP 3D
B
dsTfap2c
Late 8-cell
8-16 cell
Early 16-cell
t=10
t=13
t=20
E
Late 8-cell stage
Number of polarized cells
****
*
***
dsGFP
dsTfap2c
dsTead4
dsTT
C
dsTead4
Late 8-cell
8-16 cell
Early 16-cell
t=1
t=5
t=14
D
dsTfap2c+dsTead4
Late 8-cell
8-16 cell
Early 16-cell
t=13
t=22
t=28
F
Early 16-cell stage
Number of polarized cells
ns
****
G
F-actinPard6
F-actinPard6 3D
Ezrin-RFP
Ezrin-RFP 3D
dsGFP
dsTT
H
Ezrin apical enrichment
****
dsGFP
dsTT
I
Cas9 only
Cas9+sgRNAs
dsRNA
sgRNA1,2,3
Tfap2c genomic region
sgRNA1,2,4
Tead4 genomic region
J
Cas9 only
Tfap2c-null
Tead4-null
Tfap2c-null
Tead4-null
Tfap2c
Tead4
Ezrin DAPI
K
Polarized cell
Non-polarized cell
Percentage (%)
****
ns
****
358
152
56
62
54
27
51
Cas9 only
Tfap2c-null
Tead4-null
Tfap2c-null
Tead4-null
L
Ezrin apical enrichment
****
***
**
Cas9 only
Tfap2c-null
Tead4-null
Tfap2c-null
Tead4-null

Figure 3

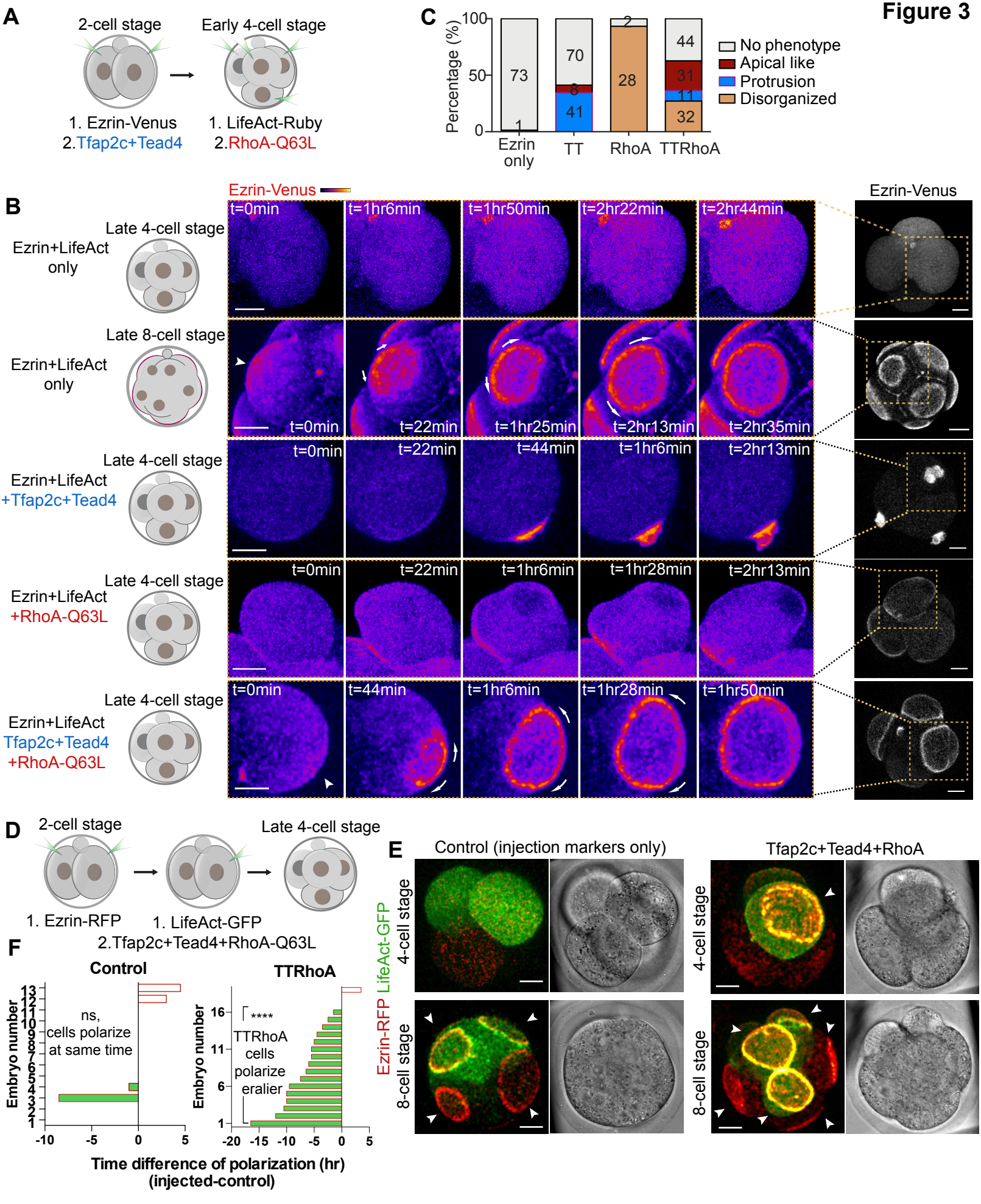
A
2-cell stage
Early 4-cell stage
1. Ezrin-Venus
2.Tfap2c+Tead4
1. LifeAct-Ruby
2.RhoA-Q63L
C
Percentage (%)
100
50
0
73
1
70
8
41
2
28
44
31
11
32
Ezrin only
TT
RhoA
TTRhoA
No phenotype
Apical like
Protrusion
Disorganized
B
Ezrin-Venus
Ezrin-Venus
Late 4-cell stage
Ezrin+LifeAct only
t=0min
t=1hr6min
t=1hr50min
t=2hr22min
t=2hr44min
Late 8-cell stage
Ezrin+LifeAct only
t=0min
t=22min
t=1hr25min
t=2hr13min
t=2hr35min
Late 4-cell stage
Ezrin+LifeAct +Tfap2c+Tead4
t=0min
t=22min
t=44min
t=1hr6min
t=2hr13min
Late 4-cell stage
Ezrin+LifeAct +RhoA-Q63L
t=0min
t=22min
t=1hr6min
t=1hr28min
t=2hr13min
Late 4-cell stage
Ezrin+LifeAct Tfap2c+Tead4 +RhoA-Q63L
t=0min
t=44min
t=1hr6min
t=1hr28min
t=1hr50min
D
2-cell stage
Late 4-cell stage
1. Ezrin-RFP
1. LifeAct-GFP
2.Tfap2c+Tead4+RhoA-Q63L
E
Control (injection markers only)
Tfap2c+Tead4+RhoA
LifeAct-GFP
Ezrin-RFP
4-cell stage
8-cell stage
F
Control
TTRhoA
ns, cells polarize at same time
****
TTRhoA cells polarize eralier
Embryo number
Time difference of polarization (hr) (injected-control)

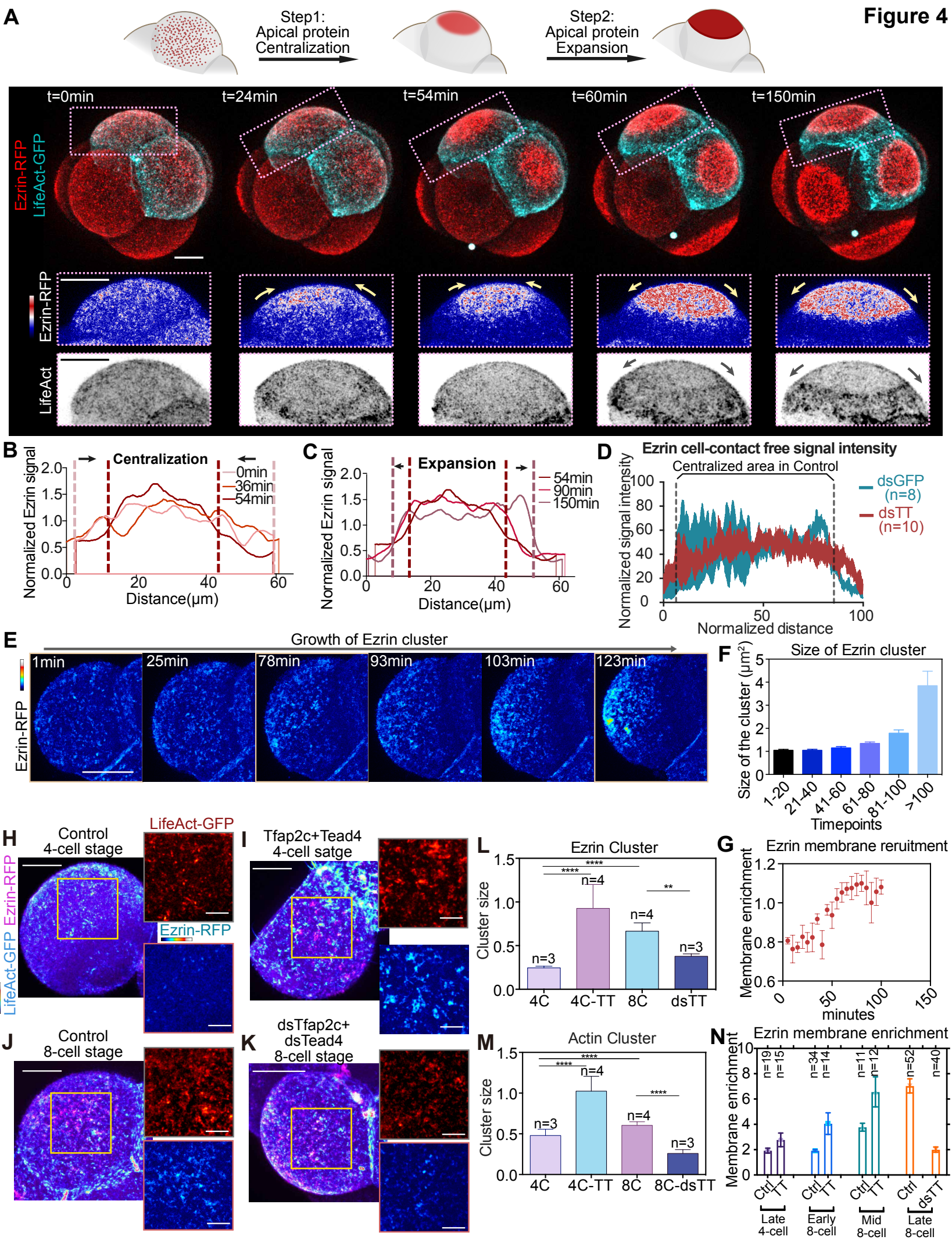
A
Step1:
Apical protein
Centralization
Step2:
Apical protein
Expansion
t=0min
t=24min
t=54min
t=60min
t=150min
Ezrin-RFP
LifeAct-GFP
Ezrin-RFP
LifeAct
B
Centralization
Normalized Ezrin signal
0min
36min
54min
Distance(μm)
C
Expansion
Normalized Ezrin signal
54min
90min
150min
Distance(μm)
D
Ezrin cell-contact free signal intensity
Centralized area in Control
Normalized signal intensity
dsGFP
(n=8)
dsTT
(n=10)
Normalized distance
E
Growth of Ezrin cluster
1min
25min
78min
93min
103min
123min
Ezrin-RFP
F
Size of Ezrin cluster
Size of the cluster (μm²)
1-20
21-40
41-60
61-80
81-100
>100
Timepoints
H
Control
4-cell stage
LifeAct-GFP
Ezrin-RFP
LifeAct-GFP Ezrin-RFP
I
Tfap2c+Tead4
4-cell satge
J
Control
8-cell stage
K
dsTfap2c+
dsTead4
8-cell stage
L
Ezrin Cluster
Cluster size
n=3
n=4
n=4
n=3
4C
4C-TT
8C
dsTT
G
Ezrin membrane reruitment
Membrane enrichment
minutes
M
Actin Cluster
Cluster size
n=3
n=4
n=4
n=3
4C
4C-TT
8C
8C-dsTT
N
Ezrin membrane enrichment
Membrane enrichment
n=19
n=15
n=34
n=14
n=11
n=12
n=52
n=40
Ctrl
TT
Ctrl
TT
Ctrl
TT
Ctrl
dsTT
Late
4-cell
Early
8-cell
Mid
8-cell
Late
8-cell

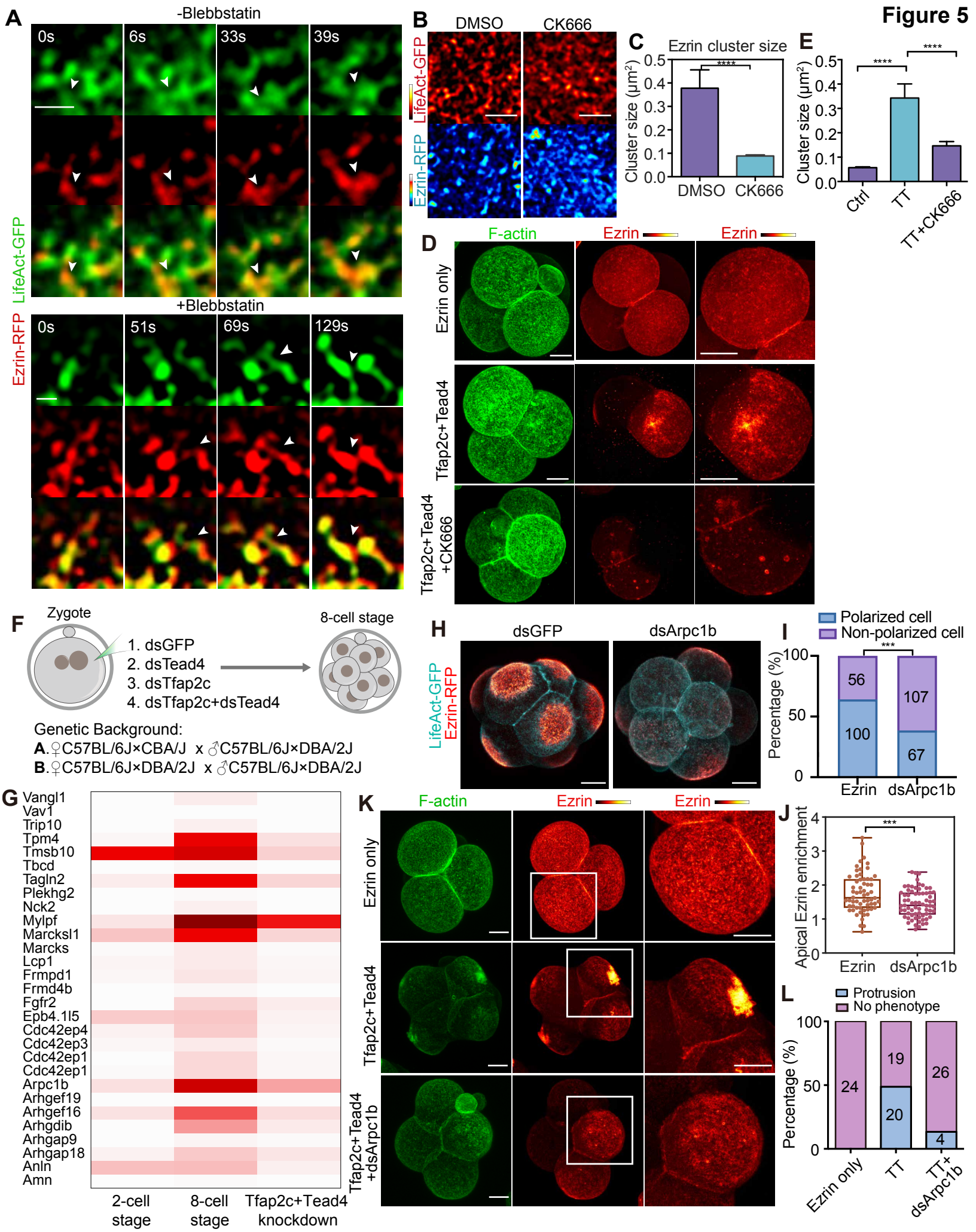
A
-Blebbstatin
0s
6s
33s
39s
LifeAct-GFP
Ezrin-RFP
+Blebbstatin
0s
51s
69s
129s
B
DMSO
CK666
LifeAct-GFP
Ezrin-RFP
C
Ezrin cluster size
Cluster size (μm²)
0.5
0.4
0.3
0.2
0.1
0.0
****
DMSO
CK666
E
Cluster size (μm²)
****
****
Ctrl
TT
TT+CK666
D
F-actin
Ezrin
Ezrin
Ezrin only
Tfap2c+Tead4
Tfap2c+Tead4 +CK666
F
Zygote
8-cell stage
1. dsGFP
2. dsTead4
3. dsTfap2c
4. dsTfap2c+dsTead4
Genetic Background:
A.♀C57BL/6J×CBA/J x ♂C57BL/6J×DBA/2J
B.♀C57BL/6J×DBA/2J x ♂C57BL/6J×DBA/2J
H
dsGFP
dsArpc1b
LifeAct-GFP
Ezrin-RFP
I
Polarized cell
Non-polarized cell
***
Percentage (%)
100
50
0
56
100
107
67
Ezrin
dsArpc1b
G
Vangl1
Vav1
Trip10
Tpm4
Tmsb10
Tbcd
Tagln2
Plekhg2
Nck2
Mylpf
Marcksl1
Marcks
Lcp1
Frmpd1
Frmd4b
Fgfr2
Epb4.1l5
Cdc42ep4
Cdc42ep3
Cdc42ep1
Cdc42ep1
Arpc1b
Arhgef19
Arhgef16
Arhgdib
Arhgap9
Arhgap18
Anln
Amn
2-cell stage
8-cell stage
Tfap2c+Tead4 knockdown
K
F-actin
Ezrin
Ezrin
Ezrin only
Tfap2c+Tead4
Tfap2c+Tead4 +dsArpc1b
J
***
Apical Ezrin enrichment
4
3
2
1
0
Ezrin
dsArpc1b
L
Protrusion
No phenotype
Percentage (%)
100
50
0
24
19
20
26
4
Ezrin only
TT
TT+ dsArpc1b

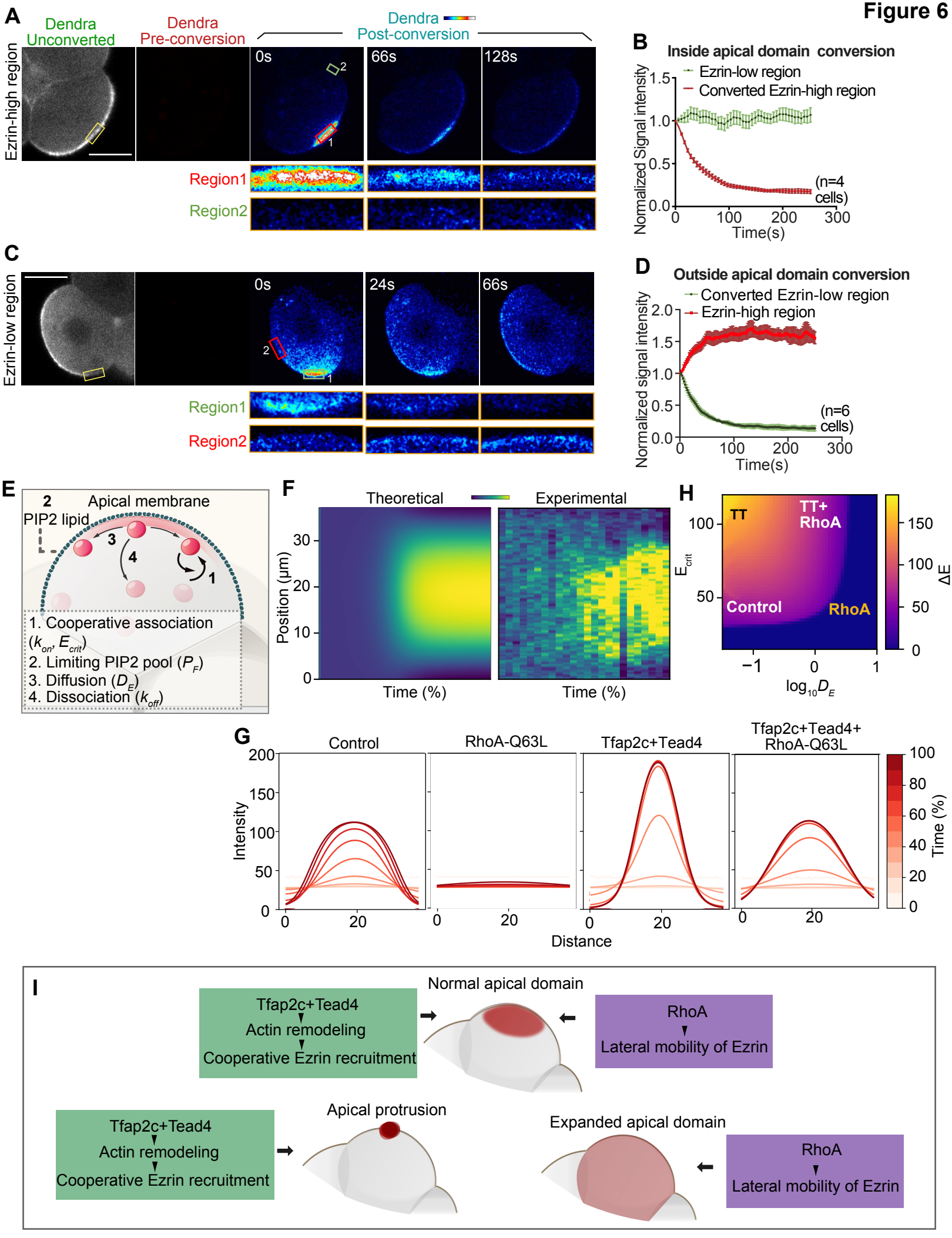
A
Dendra Unconverted
Dendra Pre-conversion
Dendra Post-conversion
Ezrin-high region
0s
66s
128s
Region1
Region2
B
Inside apical domain conversion
Ezrin-low region
Converted Ezrin-high region
Normalized Signal intensity
(n=4 cells)
Time(s)
C
Ezrin-low region
0s
24s
66s
Region1
Region2
D
Outside apical domain conversion
Converted Ezrin-low region
Ezrin-high region
Normalized signal intensity
(n=6 cells)
Time(s)
E
Apical membrane
PIP2 lipid
1. Cooperative association (k_{on}, E_{crit})
2. Limiting PIP2 pool (P_F)
3. Diffusion (D_E)
4. Dissociation (k_{off})
F
Theoretical
Experimental
Position (μm)
Time (%)
H
TT
TT+ RhoA
Control
RhoA
E_{crit}
$\log_{10}D_E$
ΔE
G
Control
RhoA-Q63L
Tfap2c+Tead4
Tfap2c+Tead4+ RhoA-Q63L
Intensity
Distance
Time (%)
I
Tfap2c+Tead4
Actin remodeling
Cooperative Ezrin recruitment
Normal apical domain
RhoA
Lateral mobility of Ezrin
Tfap2c+Tead4
Actin remodeling
Cooperative Ezrin recruitment
Apical protrusion
Expanded apical domain
RhoA
Lateral mobility of Ezrin